AGU PUBLICATIONS

Water Resources Research

RESEARCH ARTICLE
10.1002/2014WR016192

A new frequency domain analytical solution of a cascade of diffusive channels for flood routing

Luigi Cimorelli[1], Luca Cozzolino[2], Renata Della Morte[2], Domenico Pianese[1], and Vijay P. Singh[3]

[1]Dipartimento di Ingegneria Civile, Edile e Ambientale, Università degli Studi di Napoli Federico II, Napoli, Italy, [2]Centro Direzionale di Napoli, Dipartimento di Ingegneria, Università degli Studi di Napoli Parthenope, Napoli, Italy, [3]Department of Biological and Agricultural Engineering and Zachry Department of Civil Engineering, Texas A&M University, College Station, Texas, USA

Key Points:
- Frequency domain analytical solution
- Nonuniform channel geometry and downstream boundary condition are accounted
- Fast computation due to model unconditional stability

Correspondence to:
L. Cimorelli,
luigi.cimorelli@unina.it

Citation:
Cimorelli, L., L. Cozzolino, R. Della Morte, D. Pianese, and V. P. Singh (2015), A new frequency domain analytical solution of a cascade of diffusive channels for flood routing, *Water Resour. Res.*, *51*, 2393–2411, doi:10.1002/2014WR016192.

Received 24 JUL 2014
Accepted 12 MAR 2015
Accepted article online 18 MAR 2015
Published online 11 APR 2015

Abstract Simplified flood propagation models are often employed in practical applications for hydraulic and hydrologic analyses. In this paper, we present a new numerical method for the solution of the Linear Parabolic Approximation (LPA) of the De Saint Venant equations (DSVEs), accounting for the space variation of model parameters and the imposition of appropriate downstream boundary conditions. The new model is based on the analytical solution of a cascade of linear diffusive channels in the Laplace Transform domain. The time domain solutions are obtained using a Fourier series approximation of the Laplace Inversion formula. The new Inverse Laplace Transform Diffusive Flood Routing model (ILTDFR) can be used as a building block for the construction of real-time flood forecasting models or in optimization models, because it is unconditionally stable and allows fast and fairly precise computation.

1. Introduction

Flow routing models for flow propagation in channel networks are often obtained as simplified versions of the full De Saint Venant Equations [DSVEs). Nowadays, application of these simplified models to problems, such as real-time flood forecasting and operations management, is still common, despite the availability of powerful computing resources. This is justified by several reasons: (a) the lack of data about the channel geometry and the associated floodplains introduces numerical errors that may counter the advantage of using the complete De Saint Venant Equations; (b) in many cases, the peculiar dynamics of the flow propagation make the solution of the simplified models sufficient for practical purposes; and (c) the accurate solution of complete De Saint Venant models is very time consuming [*Cozzolino et al*., 2012]. On the other hand, simplified flood routing models may exhibit one or more of the following favorable characteristics: simplified rating curves (nonlooped) can be employed, the knowledge of just one upstream boundary condition is often required (discharge hydrograph or stage hydrograph), and the calibration of only few parameters is required; they are usually linear and errors in the input quantities are not amplified [*Singh and Woolhiser*, 1976]; the simplified models allow fast computation and hence they are particularly suited for problems in which large and repetitive computations are required, such as the optimal design of hydraulic infrastructures [*Cimorelli et al*., 2013a, 2014b; *Palumbo et al*., 2014; *Cozzolino et al.,* 2015].

The well-known Parabolic Approximation (PA) model is derived from the DSVEs by neglecting the inertial terms, while the Kinematic Wave is obtained by neglecting also the pressure terms [*Cunge et al*., 1980]. Despite the simplifications introduced, there are ranges of hydraulic conditions where satisfactory and accurate application of the PA model is found, as discussed in the scientific literature [*Ponce and Simmons*, 1977; *Ponce et al*., 1978; *Tsai*, 2003]. *Weinmann and Laurenson* [1979] showed that numerous approximate flow routing models can be regarded as linearized versions of these simplified models. Among the linear flow routing models, the Kalinin-Milyukov-Nash (KMN) reservoir cascade model [*Nash*, 1957; *Kalinin and Milyukov*, 1957], the Muskingum-Cunge (MC) model [*Cunge*, 1969], and the *Hayami* [1951] transfer function (HTF) have been widely employed for discharge forecasting for large rivers [*Singh*, 1996]. The linear models are attractive for their simplicity and because model parameters are easily related to channel characteristics and hydraulics conditions. However, it is widely recognized that the propagation of flood waves in channels is a nonlinear process, and linear models can provide only a crude approximation of real flow propagation phenomena.

In order to account for nonlinearities, it can be assumed that the flood wave propagation responds linearly to the input, but model parameters are recalculated as functions of local and instantaneous values of flow conditions during the marching-in-time of the algorithm. This idea has been incorporated into the development of a wide class of flood routing models known as multilinear models [*Keefer and McQuivey*, 1974; *Ponce and Yevjevich*, 1978; *Becker and Kundzewicz*, 1987; *Perumal*, 1992, 1994; *Camacho and Lees*, 1999; *Szilagyi*, 2003, 2006; *Perumal et al*., 2007, 2009; *Szilagyi and Laurinyecz*, 2012], and has allowed the use of all the previously mentioned simplified linear models as submodels embedded into the multilinear methodology. This shows that the study of linear models in hydrology is still of great interest, because they can be used as building blocks for the construction of nonlinear models.

The linear models derived from the PA model are particularly attractive, because they are able to take into account not only the wave celerity but also its attenuation. The Hayami linear transfer function [*Hayami*, 1951] is calculated assuming semiinfinite channel, and *Todini and Bossi* [1986] used the corresponding discrete impulse response to construct the Parabolic and Backwater (PAB) routing scheme. Later, *Cimorelli et al*. [2013b] extended the PAB in order to account for the hydraulic jumps and for pressurized flow in closed conduits. *Litrico et al*. [2010] used cumulants of the Hayami transfer function to derive a nonlinear Delayed Differential Equation (DDE) through a family of linear DDEs. The main drawback of the cited models is that in the Hayami transfer function, downstream boundary conditions are not properly taken into account. As highlighted by many authors [*Chung et al*., 1993; *Singh*, 1996; *Tsai*, 2005; *Cozzolino et al*., 2014a, 2014b; *Cimorelli et al*., 2014a], the downstream boundary condition can significantly modify the flow dynamics. *Chung et al*. [1993] presented a Laplace-Domain analytical solution of the Linear Parabolic Approximation (LPA) of DSVEs, accounting for the downstream boundary conditions in terms of discharge, while the corresponding time-domain solution was determined through a Fourier series approximation of the Laplace inversion formula [*Crump*, 1976]. An analytical solution in terms of discharge and flow depth, in both Laplace and time domains, was given in *Cimorelli et al*. [2014a], considering two different downstream boundary conditions and accounting for lateral inflow.

The cited linear flood routing models are derived under the hypothesis of prismatic channel and initial uniform steady state. A step forward in simplified modeling of the linearized DSVEs was made by *Litrico and Fromion* [2004], where the initial backwater curve was approximated by means of a cascade of prismatic pools with uniform initial conditions, and rational functions were used to fit the frequency response of the system. Of course, every new initial backwater curve requires a new fitting of the frequency response, and this can be very time consuming in multilinear approaches. *Munier et al*. [2008] considered a cascade of two prismatic channels with different flow and geometric characteristics, taking into account the downstream boundary condition. The reference backwater curve was approximated by a piecewise constant curve, and the transfer function of each channel was determined in the Laplace domain. The time-domain response was approximated by the solution of a simple ordinary differential equation, and parameters of the approximated solutions were determined by the moment matching method. This model was used to route the input hydrograph through an irrigation channel regulated by a gate or a weir at the downstream end, providing satisfactory results with respect to the numerical solution of the full DSVEs. Nevertheless, in natural rivers the geometry of cross sections can vary conspicuously along the river, and a cascade of two channels may not be sufficient for the approximation of the real flow behavior.

In this paper, we present a new spatially distributed flood routing model based on the Linearized Parabolic Approximation (LPA) of DSVEs, accounting for the space variation of model parameters and the downstream boundary condition. The new model is based on the analytical solution of a cascade of linear diffusive channels in the Laplace Transform domain, while the time-domain solution is obtained via a Fourier Series approximation of the Laplace Transform Inversion Integral [*Crump*, 1976]. The new Inverse Laplace Transform Diffusive Flood Routing (ILTDFR) model is suitable for real-time flood forecasting and optimization, because it allows fast computation and it is unconditionally stable. Moreover, it may serve as the linear submodel for a multilinear approach and hence it can be readily extended in order to account for nonlinearities in the flow propagation.

The present paper is organized as follows: first, the governing equations are briefly recalled; then the derivation of the model and the discussion of the mathematical properties of the model are presented. The model is evaluated making use of analytical and numerical reference solutions, and the results of laboratory experiments available in the literature. Finally, the paper is closed by conclusions in section 6.

2. Basic Equations

2.1. Linear Parabolic Approximation of the DSVEs

The DSVEs are usually used to describe the one-dimensional flow in open channels:

$$\begin{cases} B\dfrac{\partial h}{\partial t}+\dfrac{\partial Q}{\partial x}=0 \\ \dfrac{\partial Q}{\partial t}+\dfrac{\partial}{\partial x}\left(\dfrac{Q^2}{A}\right)+gA\left(\dfrac{\partial h}{\partial x}-S_0+J\right)=0 \end{cases}. \tag{1}$$

In equation (1), the symbols have the following meaning: x and t denote the space and time-independent variables, respectively; $h(x,t)$ is the water depth; $Q(x,t)$ is the flow discharge; $A(h,x)$ is the flow cross-section area; S_0 is the longitudinal bed slope; $J(Q,h,x)$ is the friction slope; $B(h,x)$ is the water surface width; and g is the gravity acceleration.

In many practical applications, the inertial terms are small with respect to the gravity and pressure terms, and therefore they can be neglected, giving rise to the so-called Parabolic Approximation (PA) of the DSVEs:

$$\begin{cases} B\dfrac{\partial h}{\partial t}+\dfrac{\partial Q}{\partial x}=0 \\ \dfrac{\partial h}{\partial x}-S_0+J=0 \end{cases}. \tag{2}$$

In *Cimorelli et al*. [2014a], the equations of the linear channel are obtained after the linearization of equation (2) around a steady uniform condition in a prismatic channel. Here a different approach is applied, and a nonprismatic channel with nonuniform steady state condition is considered. The steady state condition is characterized by uniform discharge Q_0, in order to satisfy the first of equation (2), while the variable flow depth $h = h_0(x)$ and the uniform discharge Q_0 satisfy together the second of equation (2) in the form

$$\frac{dh_0}{dx}-S_0+J_0=0, \tag{3}$$

where $J_0(x) = J(Q_0, h_0(x), x)$. To linearize equation (2), the unknown variables $Q(x,t)$ and $h(x,t)$ are expanded around the steady state flow conditions using the following form:

$$h(x,t)=h_0(x)+\varepsilon h'(x,t)+\varepsilon^2 h''(x,t)+\ldots, \quad Q(x,t)=Q_0+\varepsilon Q'(x,t)+\varepsilon^2 Q''(x,t)+\ldots, \tag{4}$$

Substituting equation (4) into equation (2), and neglecting the higher-order terms, the following Linear Parabolic Approximation is obtained

$$\begin{cases} B_0\dfrac{\partial \mathrm{h}'}{\partial t}+\dfrac{\partial Q'}{\partial x}=0 \\ \dfrac{\partial \mathrm{h}'}{\partial x}+\left(\dfrac{\partial J}{\partial h}\right)_0 h'+\left(\dfrac{\partial J}{\partial Q}\right)_0 Q'=0 \end{cases}. \tag{5}$$

where $B_0(x)=B(h_0(x), x)$, while $(\partial J/\partial h)_0$ and $(\partial J/\partial Q)_0$ are the derivatives $\partial J/\partial h$ and $\partial J/\partial Q$ calculated in $(Q_0, h_0(x), x)$, respectively.

The mathematical model obtained is linear, with coefficients B_0, $(\partial J/\partial h)_0$ and $(\partial J/\partial Q)_0$, variable in space. Now, let L_c be the length of the channel. If a reference abscissa $x_r \in [0, L_c]$ is assumed, together with reference values h_r and Q_r of the flow variables, then it is possible to consider a first-order Taylor expansion of the coefficients contained in equation (5), and the following system is obtained:

$$\begin{cases} B_r\dfrac{\partial \mathrm{h}'}{\partial t}+\dfrac{\partial Q'}{\partial x}=0 \\ \dfrac{\partial \mathrm{h}'}{\partial x}+\left(\dfrac{\partial J}{\partial h}\right)_r h'+\left(\dfrac{\partial J}{\partial Q}\right)_r Q'=0 \end{cases}. \tag{6}$$

where $B_r = B(h_r, x_r)$, while $(\partial J/\partial h)_r$ and $(\partial J/\partial Q)_r$ are the derivatives $\partial J/\partial h$ and $\partial J/\partial Q$ calculated in (Q_r, h_r, x_r). Note that in equation (6), it must be $Q_r = Q_0$, while h_r is the value of h at a reference point along the channel that does not necessarily coincide with the abscissa x_r.

It is easy to see that equation (6) can be turned into advection-diffusion form as follows:

$$\begin{cases} B_r \dfrac{\partial h'}{\partial t} + \dfrac{\partial Q'}{\partial x} = 0 \\ \dfrac{\partial Q'}{\partial t} + C_r \dfrac{\partial Q'}{\partial x} = D_r \dfrac{\partial^2 Q'}{\partial x^2} \end{cases}, \tag{7}$$

where

$$C_r = -\frac{1}{B_r}\left(\frac{\partial J}{\partial h}\right)_r \Big/ \left(\frac{\partial J}{\partial Q}\right)_r, \quad D_r = \frac{1}{B_r}\Big/\left(\frac{\partial J}{\partial Q}\right)_r. \tag{8}$$

Coefficient C_r is the celerity of the Linear Parabolic Approximation (LPA), while D_r is the diffusivity.

2.2. Laplace-Domain Approach for the LPA

In *Cimorelli et al*. [2014a], equation (7) is turned into dimensionless form using the transformations:

$$t^* = t/\tau, \quad x^* = x/L_c, \quad h^* = h'/h_r, \quad Q^* = Q'/Q_r, \tag{9}$$

where $\tau = L_c/C_r$ is a characteristic time. The following system is obtained:

$$\begin{cases} \beta \dfrac{\partial \mathrm{h}^*}{\partial t^*} + \dfrac{\partial Q^*}{\partial x^*} = 0 \\ \dfrac{\partial \mathrm{h}^*}{\partial x^*} + r_1 Q^* + r_2 \mathrm{h}^* = 0 \end{cases}, \tag{10}$$

where

$$\beta = \frac{h_r}{Q_r} B_r C_r; \quad r_1 = L_c \left(\frac{\partial \mathrm{J}}{\partial Q}\right)_r \frac{Q_r}{h_r}; \quad r_2 = \left(\frac{\partial \mathrm{J}}{\partial h}\right)_r L_c. \tag{11}$$

Application of the Laplace transform to equation (10) with the initial conditions $h^*(x^*,0) = 0$ and $Q^*(x^*,0) = 0$ leads to

$$\begin{cases} \dfrac{\partial \widehat{Q}}{\partial x^*} + \beta s^* \widehat{\mathrm{h}} = 0 \\ \dfrac{\partial \widehat{\mathrm{h}}}{\partial x^*} + r_1 \widehat{Q} + r_2 \widehat{\mathrm{h}} = 0 \end{cases}, \tag{12}$$

where s^* is the Laplace counterpart of the dimensionless time variable t^*, while $\hat{Q}$ and $\hat{h}$ are the Laplace transforms of Q^* and h^*, respectively. In the following, the *hat* symbol will be used to indicate the Laplace transform of a time-domain function $y(t)$, i.e., $\hat{y}(s) = L[y(t)]$ where $L[\bullet]$ is the Laplace transform operator. The Laplace-domain general solution of equation (12) has the form

$$\begin{bmatrix} \widehat{Q}(x^*, s^*) \\ \widehat{h}(x^*, s^*) \end{bmatrix} = \gamma(x^*, s^*) \begin{bmatrix} \widehat{Q}(0, s^*) \\ \widehat{h}(0, s^*) \end{bmatrix}, \tag{13}$$

and the expression of the state transition matrix $\gamma(x^*, s^*)$ is given in *Cimorelli et al*. [2014a]. From a mathematical point of view, the components of the matrix $\gamma(x^*, s^*)$ can be regarded as the Laplace-domain response at a given abscissa x^* caused by the unit impulses of discharge and flow depth applied at the upstream end.

3. Laplace-Domain Solution for the Cascade of Diffusive Channels

Following *Litrico and Fromion* [2004] and *Munier et al*. [2008], the case of nonuniform reference flow conditions is approximated by means of a cascade of uniform channels characterized by different parameters. In this section, this approach is generalized, and the Laplace-domain solution of the cascade of diffusive channels is presented and discussed.

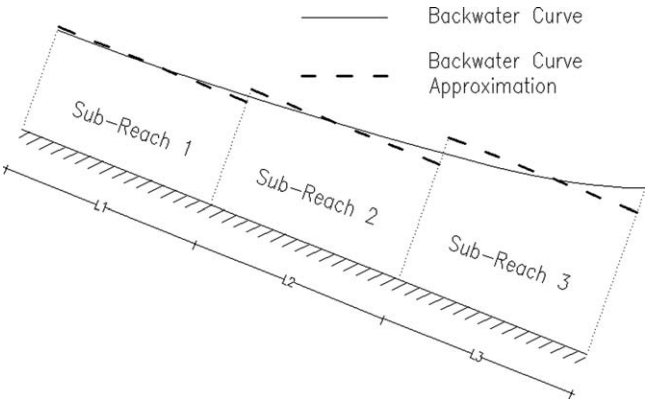

Figure 1. Nonuniform channel approximation.

3.1. Nonuniform Channel State Transition Matrix

In a channel of length L_c, the physical domain is subdivided into N adjacent intervals $S_j = [x_{j-1}, x_j]$ (with $j = 1, 2, \ldots, N$), whose length is $L_j = x_j - x_{j-1}$. The following congruency conditions are assumed:

$$x_0 = 0, \quad x_N = L_c, \quad \sum_{j=1}^{L} L_j = L_c. \tag{14}$$

In order to cope with the case of a nonuniform linear diffusive channel, the reference backwater curve is approximated with a piecewise constant curve, as shown in Figure 1. In particular, local reference flow conditions, characterized by discharge $Q_{r,j}$, flow depth $h_{r,j}$, width $B_{r,j}$, friction slope derivatives $(\partial J/\partial Q)_{r,j}$ and $(\partial J/\partial h)_{r,j}$, are assumed in each subreach S_j.

If the local dimensionless coordinate is defined as $x_j^* = (x - x_{j-1})/L_j$, with $x_j^* = 0$ for $x^* = x_{j-1}$, and $x_j^* = 1$ for $x^* = x_j$, then equation (13) can be written for the jth subreach of the channel cascade as

$$\begin{bmatrix} \widehat{Q}_j(x^*, s) \\ \widehat{h}_j(x^*, s) \end{bmatrix} = \gamma_j(x^*, s) \begin{bmatrix} \widehat{Q}_j(0, s) \\ \widehat{h}_j(0, s) \end{bmatrix}, \tag{15}$$

where $\widehat{Q}_j(x^*, s)$ and $\widehat{h}_j(x^*, s)$ are the complex flow rate and water depth variations along the jth subreach, respectively. Note that the Laplace counterpart s of the time variable t is used, instead of the Laplace counterpart s^* of the dimensionless time variable t^*, and this is needed to ensure time congruency and causality when the local uniform channel solutions are assembled in order to obtain the nonuniform channel solution. The local transition matrix is then defined as

$$\gamma_j\left(x_j^*, s\right) = \begin{bmatrix} \gamma_{j,11}\left(x_j^*, s\right) & \gamma_{j,12}\left(x_j^*, s\right) \\ \gamma_{j,21}\left(x_j^*, s\right) & \gamma_{j,22}\left(x_j^*, s\right) \end{bmatrix} = \begin{bmatrix} \dfrac{\lambda_{1,j} e^{\lambda_{2,j} x_j^*} - \lambda_{2,j} e^{\lambda_{1,j} x_j^*}}{\lambda_{1,j} - \lambda_{2,j}} & \dfrac{Q_{r,j}}{h_{r,j}} \beta_j \tau_j s \dfrac{e^{\lambda_{2,j} x_j^*} - e^{\lambda_{1,j} x_j^*}}{\lambda_{1,j} - \lambda_{2,j}} \\ \dfrac{h_{r,j}}{Q_{r,j}} \dfrac{\lambda_{1,j}\lambda_{2,j}}{\beta_j \tau_j s} \dfrac{e^{\lambda_{1,j} x_j^*} - e^{\lambda_{2,j} x_j^*}}{\lambda_{1,j} - \lambda_{2,j}} & \dfrac{\lambda_{1,i} e^{\lambda_{1,j} x_j^*} - \lambda_{2,j} e^{\lambda_{2,j} x_j^*}}{\lambda_{1,j} - \lambda_{2,j}} \end{bmatrix} \tag{16}$$

where

$$\lambda_{1,j} = \left(Pe_j - \sqrt{Pe_j^2 + 4s\tau_j Pe_j}\right)/2, \ \lambda_{2,j} = \left(Pe_j + \sqrt{Pe_j^2 + 4s\tau_j Pe_j}\right)/2. \tag{17}$$

In equations (16) and (17), the local Péclét number $Pe_j = C_{r,j} L_j / D_{r,j}$, and parameters, τ_j and β_j, are evaluated with respect to the jth subreach reference flow conditions. From equation (13), it is clear that the flow conditions at the ends of the jth subreach are connected by the equation:

$$\begin{bmatrix} \widehat{Q}_j(1, s) \\ \widehat{h}_j(1, s) \end{bmatrix} = \gamma_j(1, s) \begin{bmatrix} \widehat{Q}_j(0, s) \\ \widehat{h}_j(0, s) \end{bmatrix}. \tag{18}$$

The continuity of discharge and flow depth disturbances through the interfaces between subreaches S_{j-1} and S_j is assumed as internal boundary condition, and then it is possible to write:

$$\begin{bmatrix} \widehat{Q}_{j-1}(1, s) \\ \widehat{h}_{j-1}(1, s) \end{bmatrix} = \begin{bmatrix} \widehat{Q}_j(0, s) \\ \widehat{h}_j(0, s) \end{bmatrix}. \tag{19}$$

If equation (18) is applied recursively using the internal boundary conditions of equation (19), the general response of the nonuniform channel at the end cross section of the jth subreach can be calculated by means of

$$\begin{bmatrix} \widehat{Q}_j(1,s) \\ \widehat{h}_j(1,s) \end{bmatrix} = \gamma_c^{(j)}(s) \begin{bmatrix} \widehat{Q}_1(0,s) \\ \widehat{h}_1(0,s) \end{bmatrix}, \tag{20}$$

where the nonuniform state transition matrix is defined by

$$\gamma_c^{(j)}(s) = \prod_{r=1}^{j} \gamma_{j-r+1}(1,s). \tag{21}$$

The product in equation (21) can be immediately calculated as $\gamma_c^{(j)}(s) = \gamma_j(1,s)\,\gamma_c^{(j-1)}(s)$ if $\gamma_c^{(j-1)}(s)$ is known, and the real and imaginary parts of its components are reported in Appendix A. It is easy to show that the determinant $\|\gamma_c^{(j)}(s)\| = \gamma_{c,11}^{(j)}(s)\,\gamma_{c,22}^{(j)}(s) - \gamma_{c,12}^{(j)}(s)\,\gamma_{c,21}^{(j)}(s)$ of $\gamma_c^{(j)}(s)$ can be expressed as

$$\|\gamma_c^{(j)}(s)\| = \prod_{r=1}^{j} \exp[Pe_r]. \tag{22}$$

For $j = N$, equation (20) can be particularized as

$$\begin{bmatrix} \widehat{Q}_N(1,s) \\ \widehat{h}_N(1,s) \end{bmatrix} = \gamma_c^{(N)}(s) \begin{bmatrix} \widehat{Q}_1(0,s) \\ \widehat{h}_1(0,s) \end{bmatrix}, \tag{23}$$

and matrix $\gamma_c^{(N)}(s)$ relates the discharge and flow depth disturbances at the downstream end of the nonuniform channel with the disturbances at the upstream end. Equation (23) can be rewritten as a system of two equations as follows:

$$\begin{cases} \widehat{Q}_N(1,s) = \gamma_{c,11}^{(N)}(s)\,\widehat{Q}_1(0,s) + \gamma_{c,12}^{(N)}(s)\,\widehat{h}_1(0,s) \\ \widehat{h}_N(1,s) = \gamma_{c,21}^{(N)}(s)\,\widehat{Q}_1(0,s) + \gamma_{c,22}^{(N)}(s)\,\widehat{h}_1(0,s) \end{cases}, \tag{24}$$

where $\gamma_{c,lr}^{(N)}(s)$ are the components of matrix $\gamma_c^{(N)}(s)$. In the Laplace domain, coefficients $\gamma_{c,11}^{(N)}(s)$ and $\gamma_{c,12}^{(N)}(s)$ represent the discharge response at the downstream end of the channel due to the discharge and flow depth unit impulses, respectively, at the upstream end of the channel. Similarly, coefficients $\gamma_{c,21}^{(N)}(s)$ and $\gamma_{c,22}^{(N)}(s)$ represent the flow depth response at the downstream end of the channel due to the discharge and flow depth unit impulses, respectively, at the upstream end of the channel.

3.2. Downstream Boundary Condition and Impulse Response at the End of the Channel

The use of equation (23) requires the specification of both discharge and flow depth at the upstream end of the channel. When a downstream boundary condition is available, matrix $\gamma_c^{(N)}(s)$ can be modified in order to incorporate this additional knowledge and reduce the information needed upstream. The ability to take into account downstream boundary conditions, such as gates, orifices, and weirs, is required for the representativeness and the physical congruency of the calculations [*Cozzolino et al.*, 2014a, 2014b], but this problem is usually underestimated in simplified flow modeling [*Cimorelli et al.*, 2014a]. We assume that a stage-discharge relationship f_B between discharge Q and flow depth h is established at the downstream end of the channel:

$$Q(L_c,t) = f_B[h(L_c,t)]. \tag{25}$$

The linearization of equation (25) and the successive Laplace transform lead to

$$\widehat{Q}_N(1,s) = k_B\,\widehat{h}_N(1,s), \tag{26}$$

where

$$k_B = \frac{df_B}{dh}(h_{r,N}). \tag{27}$$

For design or simulation purposes, runoff models are often used to evaluate the discharge entering into a reach, and this hydrograph is used as upstream boundary condition $Q(0,t)$ of the wave propagation model. For this reason, it is useful to obtain the analytical expressions of the downstream response for a given

upstream discharge hydrograph. If $\widehat{Q}_1(0,s)$ is the Laplace transform of $Q(0,t)$, the substitution of equation (26) into equation (24) and the elimination of $\widehat{h}_1(0,s)$ leads after some algebra to

$$\begin{bmatrix} \widehat{Q}_N(1,s) \\ \widehat{h}_N(1,s) \end{bmatrix} = \begin{bmatrix} \hat{f}_Q^{(N)}(s) \\ \hat{g}_Q^{(N)}(s) \end{bmatrix} \widehat{Q}_1(0,s), \tag{28}$$

where $\hat{f}_Q^{(N)}(s)$ and $\hat{g}_Q^{(N)}(s)$ are defined as

$$\hat{f}_Q^{(N)}(s) = k_B \frac{\|\gamma_c^{(N)}(s)\|}{k_B \gamma_{c,22}^{(N)}(s) - \gamma_{c,12}^{(N)}(s)}, \quad \hat{g}_Q^{(N)}(s) = \frac{\hat{f}_Q^{(N)}(s)}{k_B}. \tag{29}$$

Functions $\hat{f}_Q^{(N)}(s)$ and $\hat{g}_Q^{(N)}(s)$ are the Laplace-domain transfer functions at the downstream end of the non-uniform linear diffusive channel in terms of discharge and flow depth variations, respectively, when a discharge-hydrograph is assumed as the upstream boundary condition. The formulas for the calculation of real and imaginary parts of the Laplace-domain transfer functions $\hat{f}_Q^{(N)}(s)$ and $\hat{g}_Q^{(N)}(s)$ are presented in Appendix B.

Usually, discharge measurements in rivers are obtained indirectly from flow depth measurements. For this reason, the ability of routing an upstream stage hydrograph $h(0,t)$ can come in handy in real-time flood forecasting applications. If $\widehat{h}_1(0,s)$ is the Laplace transform of $h(0,t)$, the substitution of equation (26) into equation (24) and the elimination of $\widehat{Q}_1(0,s)$ lead after some algebra to

$$\begin{bmatrix} \widehat{Q}_N(1,s) \\ \widehat{h}_N(1,s) \end{bmatrix} = \begin{bmatrix} \hat{f}_h^{(N)}(s) \\ \hat{g}_h^{(N)}(s) \end{bmatrix} \hat{h}_1(0,s), \tag{30}$$

where $\hat{f}_h^{(N)}(s)$ and $\hat{g}_h^{(N)}(s)$ are defined as

$$\hat{f}_h^{(N)}(s) = k_B \frac{\|\gamma_c^{(N)}(s)\|}{\gamma_{c,11}^{(N)}(s) - k_B \gamma_{c,21}^{(N)}(s)}, \quad \hat{g}_h^{(N)}(s) = \frac{\hat{f}_h^{(N)}(s)}{k_B}. \tag{31}$$

Functions $\hat{f}_h^{(N)}(s)$ and $\hat{g}_h^{(N)}(s)$ are the Laplace-domain transfer functions at the downstream end of the non-uniform linear diffusive channel in terms of discharge and flow depth variations, respectively, when a stage hydrograph is assumed as the upstream boundary condition.

The formulas for the calculation of real and imaginary parts of the Laplace-domain transfer functions $\hat{f}_h^{(N)}(s)$ and $\hat{g}_h^{(N)}(s)$ are presented in Appendix B.

3.3. Impulse Response at the Interfaces Between Subreaches

In order to obtain the Laplace analytical solution at the intermediate cross sections, we observe that the inversion of equation (18) and substitution in equation (19) leads to:

$$\begin{bmatrix} \widehat{Q}_{j-1}(1,s) \\ \widehat{h}_{j-1}(1,s) \end{bmatrix} = \gamma_j^{-1}(1,s) \begin{bmatrix} \widehat{Q}_j(1,s) \\ \widehat{h}_j(1,s) \end{bmatrix}. \tag{32}$$

Repeated application of equation (32) leads to:

$$\begin{bmatrix} \widehat{Q}_j(1,s) \\ \widehat{h}_j(1,s) \end{bmatrix} = \prod_{r=j+1}^{N} \gamma_r^{-1}(1,s) \begin{bmatrix} \widehat{Q}_N(1,s) \\ \widehat{h}_N(1,s) \end{bmatrix}. \tag{33}$$

In this manner, the general expression of the response at the interface between subreaches S_j and S_{j-1} can be easily found if the Laplace-domain solution $\left[\hat{Q}_N(1,s) \quad \hat{h}_N(1,s)\right]^T$ at the end of the channels cascade is known.

If the discharge-hydrograph $Q(0,t)$ is assigned as upstream boundary condition, the substitution of equation (28) into equation (33) leads to:

$$\begin{bmatrix} \widehat{Q}_j(1,s) \\ \widehat{h}_j(1,s) \end{bmatrix} = \begin{bmatrix} \hat{f}_Q^{(j)}(s) \\ \hat{g}_Q^{(j)}(s) \end{bmatrix} \widehat{Q}_1(0,s). \tag{34}$$

where

$$\begin{bmatrix} \hat{f}_Q^{(j)}(s) \\ \hat{g}_Q^{(j)}(s) \end{bmatrix} = \prod_{r=j+1}^{N} \gamma_r^{-1}(1,s) \begin{bmatrix} \hat{f}_Q^{(N)}(s) \\ \hat{g}_Q^{(N)}(s) \end{bmatrix}, \quad j=1,2,\ldots,N-1. \tag{35}$$

Functions $\hat{f}_Q^{(j)}(s)$ and $\hat{g}_Q^{(j)}(s)$ are the Laplace-domain transfer functions at the boundary between subreaches S_j and S_{j+1} in terms of discharge and flow depth variations, respectively, when a discharge-hydrograph is assumed as the upstream boundary condition.

Conversely, if the stage hydrograph $h(0,t)$ is assigned as the upstream boundary condition, then substitution of equation (30) into equation (33) leads to:

$$\begin{bmatrix} \widehat{Q}_j(1,s) \\ \widehat{h}_j(1,s) \end{bmatrix} = \begin{bmatrix} \hat{f}_h^{(j)}(s) \\ \hat{g}_h^{(j)}(s) \end{bmatrix} \hat{h}_1(0,s). \tag{36}$$

where

$$\begin{bmatrix} \hat{f}_h^{(j)}(s) \\ \hat{g}_h^{(j)}(s) \end{bmatrix} = \prod_{r=j+1}^{N} \gamma_r^{-1}(1,s) \begin{bmatrix} \hat{f}_h^{(N)}(s) \\ \hat{g}_h^{(N)}(s) \end{bmatrix}, \quad j=1,2,\ldots,N-1. \tag{37}$$

Functions $\hat{f}_h^{(j)}(s)$ and $\hat{g}_h^{(j)}(s)$ are the Laplace-domain transfer functions at the boundary between subreaches S_j and S_{j+1} in terms of discharge and flow depth variations, respectively, when a stage hydrograph is assumed as the upstream boundary condition.

The calculation of transfer functions $\hat{f}_Q^{(j)}(s)$, $\hat{g}_Q^{(j)}(s)$, $\hat{f}_h^{(j)}(s)$, and $\hat{g}_h^{(j)}(s)$ can be accomplished by exploiting a recursion property, as discussed in Appendix C.

3.4. Unit-Step Response in the Laplace Domain

In practical applications, realistic input hydrographs are often approximated as a sequence of rectangular pulses, and this prompts the derivation of unit-step response of the nonuniform channel. If $y(t)$ is the time-domain response of a generic linear system to the unit impulse, the corresponding unit-step response $Y(t)$ is defined as the primitive of $y(t)$. The Laplace-domain image $\hat{Y}(s)$ of $Y(t)$ can be readily obtained from the Laplace transform $\hat{y}(s)$ of $y(t)$ by exploiting the following property:

$$\hat{Y}(s) = L[Y(t)] = L\left[\int_0^t y(\tau)d\tau\right] = \frac{1}{s}\hat{y}(s). \tag{38}$$

Let $\hat{F}_Q^{(j)}(s)$ and $\hat{G}_Q^{(j)}(s)$ be the Laplace-domain unit-step responses corresponding to the transfer functions $\hat{f}_Q^{(j)}(s)$ and $\hat{g}_Q^{(j)}(s)$ ($j = 1,2,\ldots,N$), and $\hat{F}_h^{(j)}(s)$ and $\hat{G}_h^{(j)}(s)$ be the Laplace-domain unit-step responses corresponding to the transfer functions $\hat{f}_h^{(j)}(s)$ and $\hat{g}_h^{(j)}(s)$ ($j = 1,2,\ldots,N$). The real and imaginary parts of these unit-step functions are immediately calculated from the real and imaginary parts of the corresponding transfer functions, as presented in Appendix D.

4. Description of the Flood Routing Algorithm

Consider a generic linear hydrologic system whose time-domain unit-step response is the function $Y(t)$, characterized by $Y(t) = 0$ for $t \leq 0$. Starting from $t = 0$, the system is solicited by the input function $I(t)$, and this is approximated by a sequence of rectangular pulses I_k ($k = 1, 2, \ldots$) of length Δt, where

$$I_k = \frac{1}{\Delta t}\int_{(k-1)\Delta t}^{k\Delta t} I(\tau)d\tau, \tag{39}$$

is the average value of the input function during the kth time interval. The output $O(t_n)$ of the system at the generic time level $t_n = n\Delta t$ can be approximated by means of the following summation [*Chow et al.*, 1988]:

$$O(t_n)=\sum_{k=1}^{n} I_k\{Y[(n-k+1)\Delta t]-Y[(n-k)\Delta t]\}. \quad (40)$$

This formula is the basis of the ILTDFR algorithm, as it will be shown in the next subsections.

4.1. Approximation of Time-Domain Unit-Step Responses in the Time Domain

The use of equation (40) requires the availability of the time-domain unit-step responses $F_Q^{(j)}(t)=L^{-1}\left[\hat{F}_Q^{(j)}(s)\right]$, $G_Q^{(j)}(t)=L^{-1}\left[\hat{G}_Q^{(j)}(s)\right]$, $F_h^{(j)}(t)=L^{-1}\left[\hat{F}_h^{(j)}(s)\right]$, and $G_h^{(j)}(t)=L^{-1}\left[\hat{G}_h^{(j)}(s)\right]$, where $L^{-1}[\bullet]$ is the inverse Laplace Transform operator. The time-domain analytic responses can be easily calculated for the channel cascade with $N=1$ [*Cimorelli et al.*, 2014a]. However, it is hard to calculate the analytical unit-step response in the time domain for the case $N\geq 2$, and the Crump algorithm [*Crump*, 1976] can be used in order to obtain a numerical approximation.

In order to evaluate at time $t\in[0,t_{\max}]$ the Inverse Laplace Transform $Y(t)$ of a Laplace-domain function $\hat{Y}(s)$, the Crump algorithm employs the following Fourier Series approximation of the Laplace Inversion integral

$$Y(t)\cong\frac{e^{at}}{T}A_c\sum_{r=0}^{m}\left\{\mathrm{Re}\left[\hat{Y}(s_r)\right]\cos\left(\frac{r\pi}{T}t\right)-\mathrm{Im}\left[\hat{Y}(s_r)\right]\sin\left(\frac{r\pi}{T}t\right)\right\}, \quad (41)$$

where $A_c=1/2$ if $k=0$, while $A_c=1$ otherwise, $s_r=a+ir\pi/T$, and i is the imaginary unit. Parameters a and T can be evaluated as $T=1.6t_{\max}$ and $a=\ln(E')/2T$, where t_{max} denotes the simulation length and E' is the maximum relative error [*Cohen*, 2007]. The number of addends m of the summation is an odd positive integer, and increasing values of m lead to greater accuracy of the approximate formula. The epsilon algorithm [*Wynn*, 1962] is employed to accelerate the convergence of the summation.

4.2. ILTDFR Main Steps

In order to fix the ideas, let us suppose that the upstream boundary condition consists of the discharge hydrograph $Q'(0,t)$, and that the flow characteristics along the nonuniform linear channel are desired during the simulation interval of duration $t_{\max}$. The ILTDFR algorithm consists of the following steps:

1. The time interval $t_{\max}$ is subdivided into M subintervals of uniform length Δt, with $t_{\max}=M\Delta t$. The average value $Q_{0,k}$ of the input discharge during the kth time step is calculated by means of equation (39), where $I(t)=Q'(0,t)$.
2. The nonuniform channel is subdivided in N subreaches, in which local geometric and reference flow characteristics, L_j, $Q_{r,j}$, $h_{r,j}$, $(\partial J/\partial h)_r$, and $(\partial J/\partial Q)_r$, and $B_{r,j}$, are assumed. The corresponding local parameters Pe_j, τ_j, and β_j are calculated starting from these local characteristics.
3. The period $T=1.6t_{\max}$ and constant $a=\ln(E')/2T$, where E' is the admissible relative error, are defined. The components of the complex variable $s_r=a+ir\pi/T$ are calculated for $r=0, 1, 2,\ldots, m$, where m is the number of the addends used for Crump's summation.
4. The components of the local matrix $\gamma_j(1,s_r)$ can be calculated using equation (16) for $r=0, 1, 2, \ldots, m$ and $j=1, 2,\ldots, N$. The algorithm described in Appendix A is used to calculate the components of matrix $\gamma_c^{(N)}(s)$ defined by equation (21) with $j=N$, for $s=s_r$ ($r=0, 1, 2,\ldots, m$).
5. The formulas contained in Appendix B are used to calculate the components of the Laplace-domain transfer functions $\hat{f}_Q^{(N)}(s)$ and $\hat{g}_Q^{(N)}(s)$ defined by equation (29), for $s=s_r$ ($r=0, 1, 2,\ldots, m$). The formulas contained in Appendix C are used to calculate $\hat{f}_Q^{(j)}(s)$ and $\hat{g}_Q^{(j)}(s)$ defined by equation (35), for $s=s_r$ ($r=0, 1, 2,\ldots, m$) and for $j=1, 2,\ldots, N$.
6. Once $\hat{f}_Q^{(j)}(s)$ and $\hat{g}_Q^{(j)}(s)$ are known, the Laplace-domain unit-step responses $\hat{F}_Q^{(j)}(s)$ and $\hat{G}_Q^{(j)}(s)$ are calculated using the formulas of Appendix D, for $s=s_r$ ($r=0, 1, 2,\ldots, m$) and for $j=1, 2,\ldots, N-1$.
7. Equation (41), where the position $\hat{Y}(s)=\hat{F}_Q^{(j)}(s)$ is made, is used to evaluate the time-domain unit-step response $F_Q^{(j)}(t)=Y(t)$ at the time levels $t=t_k$, with $t_k=k\Delta t$ ($k=0, 1, 2, \ldots, M$). In the same manner, an approximation of the unit-step response $G_Q^{(j)}(t)$ at the same time levels is evaluated from $\hat{G}_Q^{(j)}(s)$.
8. For each time level $t_n=n\Delta t$ ($n=1, 2,\ldots, M$), the discharge at the downstream end of the subreach S_j ($j=1, 2,\ldots, N$) is evaluated by means of

$$Q(x_j, n\Delta t) = \sum_{k=1}^{n} Q_{0,k} \left\{ F_Q^{(j)}[(n-k+1)\Delta t] - F_Q^{(j)}[(n-k)\Delta t] \right\}, \quad (42)$$

while the flow depth is evaluated by means of

$$h(x_j, n\Delta t) = \sum_{k=1}^{n} Q_{0,k} \left\{ G_Q^{(j)}[(n-k+1)\Delta t] - G_Q^{(j)}[(n-k)\Delta t] \right\}. \quad (43)$$

When a stage hydrograph $h(0,t)$ is available as the upstream boundary condition, the procedure is substantially unaltered, but equations (42) and (43) are substituted by

$$Q(x_j, n\Delta t) = \sum_{k=1}^{n} h_{0,k} \left\{ F_h^{(j)}[(n-k+1)\Delta t] - F_h^{(j)}[(n-k)\Delta t] \right\}, \quad (44)$$

and

$$h(x_j, n\Delta t) = \sum_{k=1}^{n} h_{0,k} \left\{ G_h^{(j)}[(n-k+1)\Delta t] - G_h^{(j)}[(n-k)\Delta t] \right\}. \quad (45)$$

In equations (44) and (45), $h_{0,k}$ is the average value of the input flow depth during the kth time step, and the time-domain unit-step responses $F_Q^{(j)}(t)$ and $G_Q^{(j)}(t)$ are evaluated starting from the Laplace-domain impulse responses $\hat{f}_h^{(j)}(s)$ and $\hat{g}_h^{(j)}(s)$.

Note that the procedure described allows to supply the output of the system at a given time level without making use of the knowledge about the system state at the preceding instants. For this reason, the algorithm is unconditionally stable. Moreover, following the approach used by *Litrico and Fromion* [2004], it is possible to see that the algorithm proposed converges to the solution of the Linear PA with variable coefficients of equation (5), and it is first-order accurate in time and space.

5. Model Testing

In the present section, the model described in the preceding sections is tested considering two synthetic benchmarks and the results of two laboratory experiments.

5.1. Step-Response in the Linear Channel With Uniform Characteristics

The idea of the present test is to compare the solution of ILTDFR, which solves the linear PA equations, with an analytical benchmark for the same equations, taking into account the downstream boundary conditions. A natural and objective candidate for such a comparison is the unit-step response, supplied in *Cimorelli et al*. [2014a] for the uniform linear channel.

The test consists of a rectangular prismatic channel controlled by a weir at the downstream end, and its geometric characteristics are summarized as follows: $L_c = 10{,}000$ m, $B = 50$ m, $S_0 = 0.0002$ m/m. The reference discharge is $Q_r = 50$ m^3/s, and the reference flow depth h_r is the uniform flow depth corresponding to Q_r by means of the Manning formula with friction coefficient $n_M = 0.025$ m$^{-1/3}$s, while all the model parameters have been computed with respect to Q_r and h_r.

The downstream boundary condition is modeled through the weir equation:

$$Q = \mu_w B_w \sqrt{2g(h-h_w)^3}, \quad (46)$$

where $\mu_w = 0.40$ is the discharge coefficient; $B_w = B$ is the width of the weir; and $h_w = 2$ m is the weir height.

The step responses at the middle of the channel in terms of discharge deviation Q' and flow depth deviation h' are calculated considering a unit-step discharge hydrograph imposed upstream, and $N = 2$ subreaches of equal length. The results, obtained considering $m = 49$ addends of Crump's summation and $\Delta t = 100$ s, are plotted in Figure 2. Inspection of the figure shows that Crump's algorithm supplies values of the unit-step responses that are in accordance with the expected analytical solutions.

A more objective examination can be made considering Table 1, where absolute errors of the unit-step responses are summarized for different time instants. Inspection of the table shows that the order of

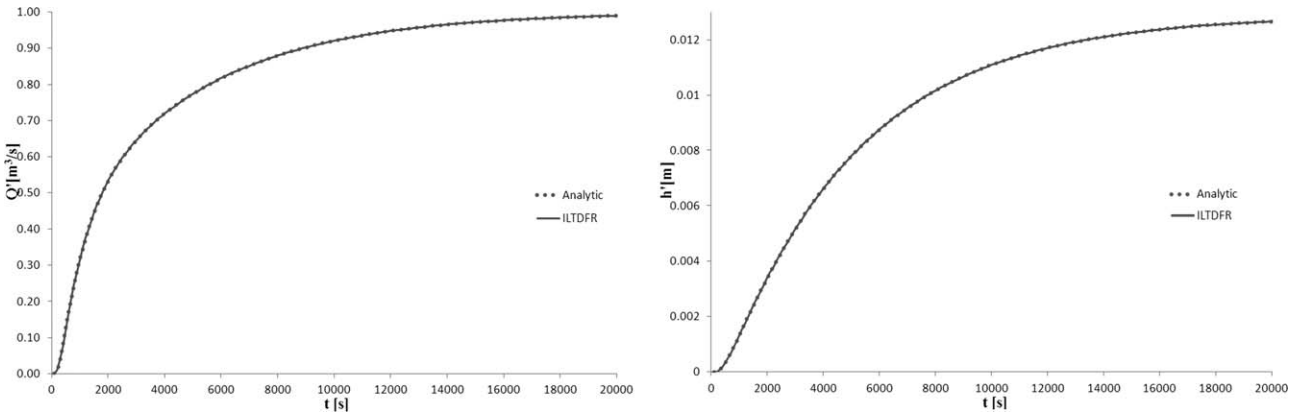

Figure 2. Comparison between analytical step responses (dots) and ILTDFR (lines) in terms of both discharge and flow depth variations.

magnitude of the error in terms of Q' is between $1\cdot\times 10^{-5}$ and $1\cdot\times 10^{-6}$ for this test-case, becoming stable for long t. Interestingly, the error in terms of h' is even smaller. The exercise is repeated for $N = 4$, 6, and 8, showing that the order of magnitude of the error does not change significantly with the number of subreaches, as shown in Table 1, and the trend of error is conserved.

From this test, it can be concluded that the idea of obtaining numerically the inverse Laplace transform of the unit-step responses supplies results that are sufficient for practical applications.

5.2. Comparison With a Nonuniform Reference Solution

The objective of the present test is to verify the ability of the ILTDFR model to converge to the solution of equation (5) with the first order of accuracy in time and space. The study case consists of a nonprismatic channel of length $L_c = 10{,}000$ m, longitudinal slope $S_0 = 0.0005$ m/m, and rectangular cross section whose width varies linearly along the channel:

$$B_s(x) = 50 + (10/L)\cdot(L - x). \tag{47}$$

A weir is present at the downstream end of the channel, and the corresponding boundary condition is described by equation (46) with $h_w = 2$ m, $\mu_w = 0.4$, and $B_w = 50$ m. The nonuniform reference condition is represented by the backwater curve corresponding to constant discharge $Q_0 = 100$ m^3/s, where the friction slope is calculated using Manning's formula with roughness coefficient $n_M = 0.02$ s m$^{-1/3}$. This condition is used to calculate along the channel the nonuniform coefficients appearing in equation (5). The upstream boundary condition is represented by the following inflow hydrograph

$$Q'(0,t) = Q'_p \frac{t}{T_p}\exp\left[1 - \frac{t}{T_p}\right], \tag{48}$$

where $Q'_p = 200$ m^3/s and $T_p = 7200$ s. Since it is hard to obtain the analytical solution of equation (5) when the coefficients are variable, a four point Preissmann finite difference scheme has been used in order to

Table 1. Uniform Channel Test[a]

N	2		4		6		8	
t (s)	Err Q′	Err h′	Err Q′	Err h′	Err Q′	Err h′	Err Q′	Err h′
100	5.08E-06	1.79E-08	5.08E-06	2.81E-09	2.90E-06	1.33E-08	2.90E-06	1.33E-08
200	7.44E-06	3.18E-08	2.40E-05	9.55E-08	3.87E-06	8.11E-09	3.87E-06	8.11E-09
500	2.59E-05	1.53E-08	2.64E-05	1.13E-08	1.63E-06	1.28E-08	1.63E-06	1.28E-08
1,000	8.31E-07	1.19E-08	1.49E-06	1.20E-08	9.96E-07	1.29E-08	9.96E-07	1.29E-08
2,000	1.00E-06	1.29E-08	1.00E-06	1.29E-08	9.99E-07	1.29E-08	9.99E-07	1.29E-08
5,000	1.00E-06	1.29E-08	1.00E-06	1.29E-08	9.99E-07	1.29E-08	9.99E-07	1.29E-08
10,000	1.00E-06	1.29E-08	1.00E-06	1.29E-08	1.00E-06	1.29E-08	1.00E-06	1.29E-08
20,000	1.00E-06	1.29E-08	1.00E-06	1.30E-08	1.06E-06	1.29E-08	1.06E-06	1.29E-08

[a]Absolute errors at the middle of the channel.

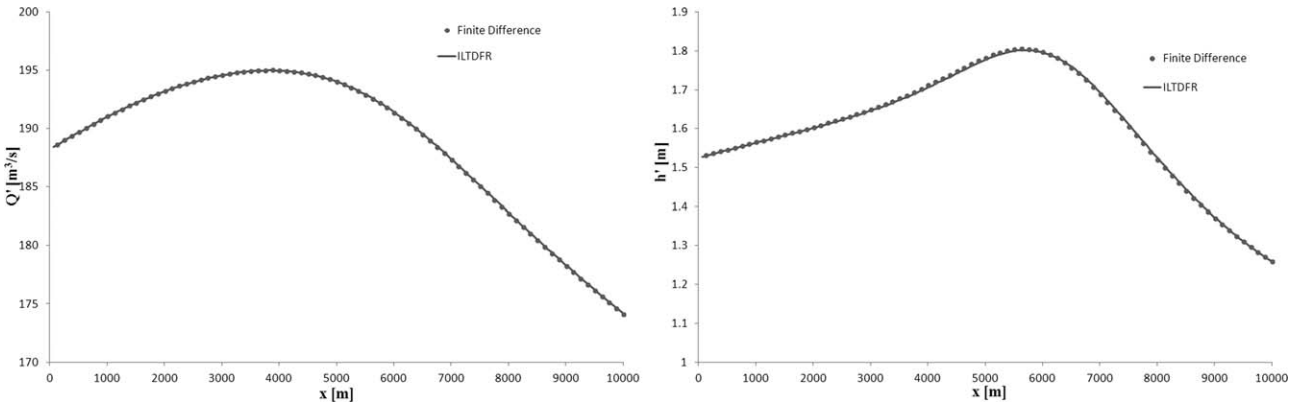

Figure 3. Comparison between finite difference solution (dots) and ILTDFR (lines) in terms of both discharge and flow depth variations at time $t = 10{,}000$ s.

produce a reference solution at time $t = 10{,}000$ s, considering a ultrafine grid with $\Delta x = 0.5$ m and $\Delta t = 0.01$ s. The corresponding solution is represented in Figure 3, with reference to the discharge flow depth variations Q' and h'.

The solution of the problem is then computed at $t = 10{,}000$ s making use of the ILTDFR model, with $N = 80$ subreaches of uniform length $L_i = 125$ m, and a time step $\Delta t = 25$ s. In each element of the channel cascade, the reference parameters are calculated averaging the corresponding quantities evaluated with reference to the initial backwater curve at the ends of each subreach. Results of the ILTDFR computations are reported in Figure 3 in terms of flow rate Q' and water depth h' disturbances, and the inspection of the figure shows that the solution provided by the ILTDFR exhibits a very good match with the solution obtained with the finite difference scheme.

Application of ILTDFR is repeated with different time steps and subreach lengths, but keeping the ratio $\Delta t/L_i$ constant, and for each of these cases, the L_∞-norm of the error is calculated with respect to the reference solution. These errors are reported in Table 2, confirming that the order of accuracy of the algorithm is the first.

5.3. Comparison With the Results of Laboratory Tests

In this test, results of the numerical model are compared with the experimental data obtained for the case of flow propagation in a compound channel [*Rashid and Chaudhry*, 1995]. The experimental setup consisted of a rectangular flume 21 m long, $b_f = 0.93$ m wide, and $H = 0.56$ m deep, with uniform longitudinal bed slope $S_0 = 0.0021$. The dimensions of the compound cross section were (see Figure 4): $b_m = 0.31$ m, $H_m = 0.20$ m, and $b_f = 0.93$ m. The Manning n_M value was dependent on the flow depth, h, as follows: 0.013 for $h \leq 0.23$ m, 0.016 for $0.23 < h \leq 0.26$ m, 0.018 for $0.26 < h \leq 0.29$ m, 0.016 for $0.29 < h \leq 0.32$ m, and 0.015 for $h > 0.32$ m. Nine gauging stations were located along the channel at different distances from the inlet, as reported in Table 3. An inclined sluice gate (whose sill position coincides with Station 9) was present at the downstream end of the laboratory flume, and the corresponding boundary condition was expressed as

Table 2. Convergence Test[a]

		$L_\infty(Q')$ (m^3/s)		$L_\infty(h')$ (m)	
L_i (m)	Δt (s)	Error	Order	Error	Order
2000	400	2.36		0.0784	
1000	200	1.01	1.22	0.0464	0.758
500	100	0.449	1.17	0.0255	0.865
250	50	0.196	1.20	0.0135	0.915
125	25	0.0919	1.09	0.00697	0.955

[a] L_∞-norms of the error.

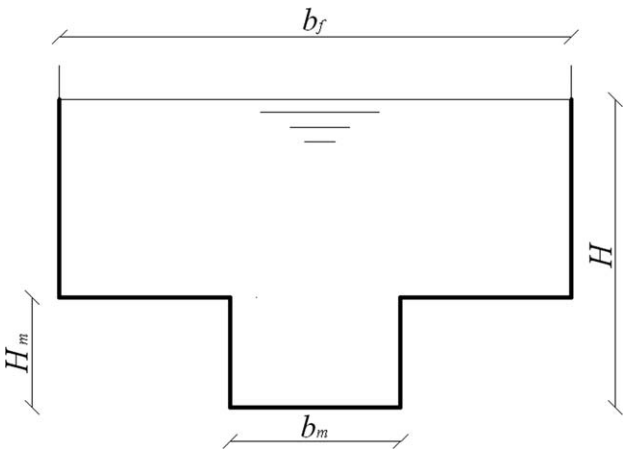

Figure 4. *Rashid and Chaudhry* [1995] experiment compound cross section.

$$Q = CH^m, \tag{49}$$

in which Q and H are the discharge and the flow depth over the gate, respectively, and the two constants, $C = 9.35$ and $m = 1.14$, were determined by *Rashid and Chaudhry* [1995] by a regression of experimental values of the pairs (H, Q). The initial conditions were represented by a steady state backwater curve, reported in *Rashid and Chaudhry* [1995].

In *Rashid and Chaudhry* [1995], two experiments are reported. In Test 1, the flow occupies the entire compound cross section, while in Test 2 the flow is contained into the central rectangular channel. In order to compare the results of ILTDFR with the laboratory results, the stage hydrograph at Station 1 is taken as the upstream boundary condition of the channel, whose downstream end is taken at the Station 9: from Table 3 it is clear that the actual operative length of the channel is $L_c = 18.6$ m.

The linear PA model is not able to take into account the nonlinearities of flow, whose effect is prevailing if long time steps and finite variations of the flow variables are considered. In order to take into account the nonlinearities of the flow in an approximate way, an acceptable strategy is to consider a reference state whose flow characteristics are intermediate between the initial and final flow conditions. In this sense, the reference values of discharge and water depth used to evaluate the local state transition matrices $\gamma_j\left(x_j^*, s\right)$ are not those corresponding to the initial steady flow. However, the final flow conditions are not known and a way to obtain a first estimate of the final flow condition is used first in the following simple calibration procedure:

1. Given the upstream stage hydrograph, the initial steady state backwater curve, and the downstream boundary condition, the upstream rating curve is derived through by a first application of ILTDFR, so that an estimate of the variation intervals for both discharge and flow depth is obtained.
2. An intermediate flow depth value (0.26 and 0.168 m for experiments 1 and 2, respectively) between the maximum and minimum flow depths derived in step 1 is chosen and the corresponding discharge (0.09 and 0.06 m^3/s for experiments 1 and 2, respectively) is fixed, while at the downstream end of the channel, the flow depth corresponding to the above mentioned discharge is evaluated with equation (49).
3. A linear variation of the flow depth between the upstream and downstream ends of the channel is assumed as reference state, and all the model parameters are evaluated with respect to this linear backwater curve.

Table 3. Laboratory Test by *Rashid and Chaudhry* [1995][a]

Gauging Station	Distance From the Inlet (m)	x (m)	Notes
1	1.22	0	Upstream boundary
2	3.35	2.13	
3	6.09	4.87	
4	7.61	6.39	
5	11.3	10.1	
6	15.2	14.0	
7	16.8	15.5	
8	18.9	17.7	
9	19.8	18.6	Inclined gate sill

[a]Position of the gauges.

The time step for the numeric calculations is equal to $\Delta t = 10$ s, while the channel is discretized making use of eight subchannels, whose length is equal to the distance between two adjacent gauging stations (see Table 3). The results of ILTDFR are compared in Figure 5 with the laboratory results corresponding to Stations 2 and 5. The same numerical tests are tackled in *Rashid and Chaudhry* [1995], where the full DSVEs are solved, and in *Perumal et al.* [2007, 2009], where two models derived from the MC model are used, and the corresponding results are reported in Figure 5 as well.

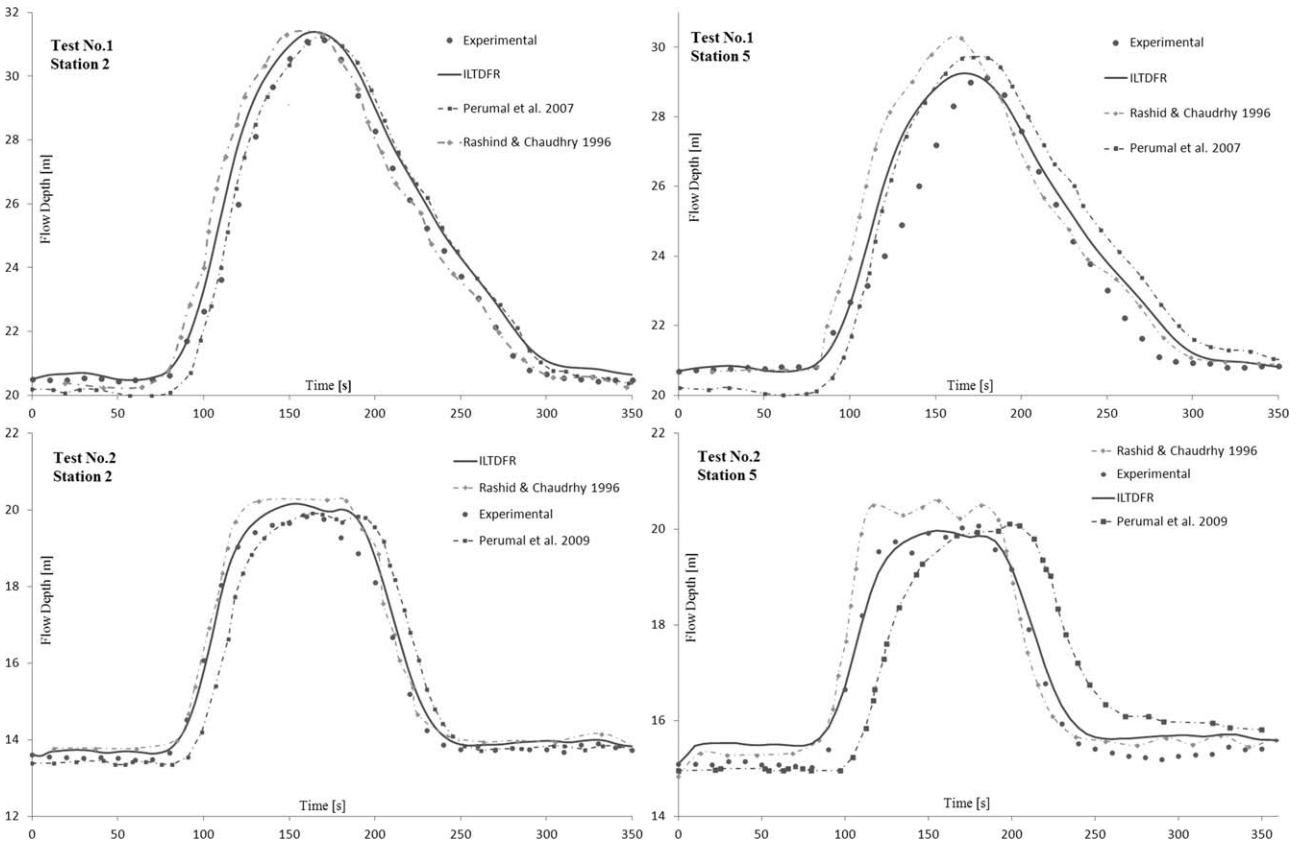

Figure 5. Comparison of ILTDFR with experimental data and numerical results obtained by *Rashid and Chaudhry* [1995] and *Perumal et al*. [2007, 2009].

With reference to Station 2 in Test1 and Test 2, and Station 5 in Test 2, it is apparent that the laboratory results are reasonably reproduced by ILTDFR. In particular, the peak flow depth and the arrival time of the wave seem to be captured with precision sufficient for practical applications. In line of principle, better results could have been obtained by ILTDFR as a linear component of a multilinear approach, but this goes beyond the scope of the present work.

The results for Station 5 during the Test 1 are not satisfactorily reproduced by ILTDFR, and this can be explained considering that the shear stress between the flow in the floodplain and the flow in the central channel is not taken into account by the model [see *Rashid and Chaudhry*, 1995]. Interestingly, this issue is shared by the numerical models presented in *Rashid and Chaudhry* [1995] and in *Perumal et al*. [2007, 2009]. In particular, the unsatisfactory results supplied by the full DSVEs model give an indirect confirmation about the fact that the linear nature of ILTDFR is not the cause of the discrepancies with the laboratory results.

In both the tests considered, Station 5 is close to the downstream end of the channel, and then the ability to capture the results at this station is an indirect confirmation of the ability of the numerical models to incorporate the boundary condition. The models by *Perumal et al*. [2007, 2009] are derived from the MC model, which is intrinsically unable to take into account the effects of the downstream boundary condition, because it is based on the Kinematic Wave approximation. Not surprisingly, ILTDFR behaves significantly better than these two models at Gauge 5, and its results are comparable to those supplied by the numerical model of *Rashid and Chaudhry* [1995], where the full DSVEs are solved.

In order to show the sensitivity of the model to the choice of the parameter, results of the simulation performed using both the initial conditions and the intermediate conditions as reference state are reported in Figure 6.

Inspection of Figure 6 shows that the flow depth at Station 5 is underestimated using the initial conditions as reference state, while it is reasonably reproduced at Station 2. Therefore, at least in this case, the initial

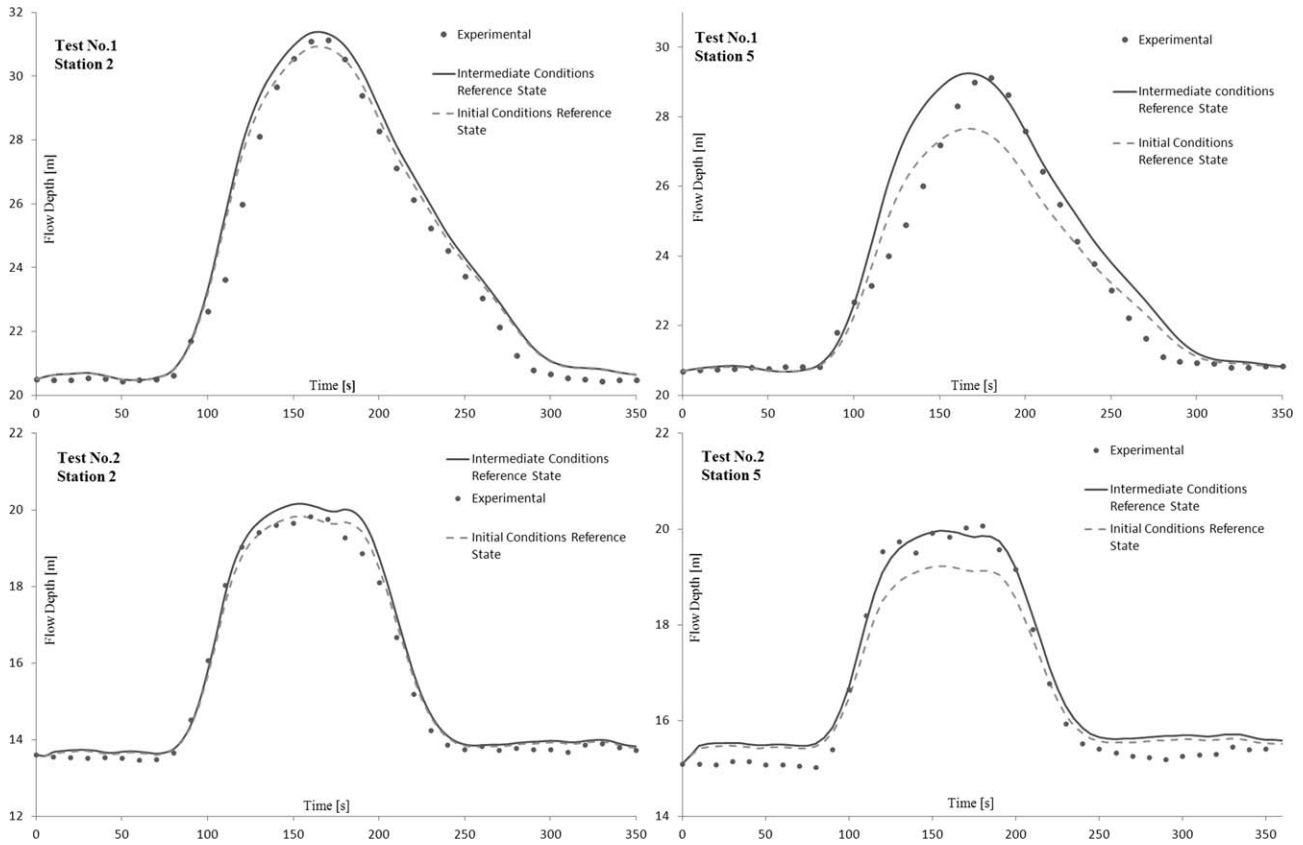

Figure 6. Comparison of the results obtained with ILTDFR using the initial flow conditions and the intermediate flow conditions as reference state.

conditions can be used as reference state in order to estimate the rating curve at the most upstream cross section. This has been done in the calibration procedure reported above.

6. Conclusions

Despite the computational power provided by the modern computers, simplified flow routing models are still widespread for real-time flood forecasting, operational management, and optimal design of hydraulic infrastructures. In this paper, it is shown how the solution of a linear Parabolic Approximation of the full De Saint Venant Equations in nonuniform channels can be approximated by a cascade of linear uniform flow diffusive channels. With reference to this approach, it is possible to construct a new flow routing model, based on the numerical inversion to the time domain of a Laplace-domain analytical solution of a diffusive channels cascade. This new Inverse Laplace Transform Diffusive Flood Routing (ILTDFR) model exhibits many favorable characteristics: the algorithm is unconditionally stable with respect to time discretization, and then very fast computations are allowed if long time steps are chosen; the cascade of uniform channels accounts for nonuniform channel geometry and hydraulic conditions in nonprismatic channels; the discharge and flow depth are computed simultaneously, and then the conservation of the variables is ensured; both stage hydrograph or discharge hydrograph boundary conditions can be imposed upstream; the model can be easily extended in order to take into account nonlinearities by adopting a multilinear approach. The numerical experiments show that the numerical approach is first-order accurate in time and space, and that the laboratory results about the propagation of flow in realistic channels are reasonably reproduced.

In line of principle, the cascade of linear diffusive channels used in the present work can be exploited to take into account distributed and concentrated lateral inflows and outflows, and the appropriate assembling of the state-transition matrices can take into account junctions. These features can allow the application of the model to complex large channel networks, and this is the objective of ongoing research.

Appendix A

Exploiting the recursion property of the nonuniform state transition matrix, the real and imaginary parts of the components of $\gamma_c^{(j)}(1,s)$ are calculated as

$$\begin{aligned}\mathrm{Re}\left[\gamma_{c,11}^{(j)}(s)\right]&=\mathrm{Re}\left[\gamma_{j,11}(1,s)\right]\mathrm{Re}\left[\gamma_{c,11}^{(j-1)}(s)\right]-\mathrm{Im}\left[\gamma_{j,11}(1,s)\right]\mathrm{Im}\left[\gamma_{c,11}^{(j-1)}(s)\right]\\&+\mathrm{Re}\left[\gamma_{j,12}(1,s)\right]\mathrm{Re}\left[\gamma_{c,21}^{(j-1)}(s)\right]-\mathrm{Im}\left[\gamma_{j,12}(1,s)\right]\mathrm{Im}\left[\gamma_{c,21}^{(j-1)}(s)\right],\end{aligned}\tag{A1}$$

$$\begin{aligned}\mathrm{Im}\left[\gamma_{c,11}^{(j)}(1,s)\right]&=\mathrm{Im}\left[\gamma_{j,11}(1,s)\right]\mathrm{Re}\left[\gamma_{c,11}^{(j-1)}(s)\right]+\mathrm{Re}\left[\gamma_{j,11}(1,s)\right]\mathrm{Im}\left[\gamma_{c,11}^{(j-1)}(s)\right]\\&+\mathrm{Im}\left[\gamma_{j,12}(1,s)\right]\mathrm{Re}\left[\gamma_{c,21}^{(j-1)}(s)\right]+\mathrm{Re}\left[\gamma_{j,12}(1,s)\right]\mathrm{Im}\left[\gamma_{c,21}^{(j-1)}(s)\right],\end{aligned}\tag{A2}$$

$$\begin{aligned}\mathrm{Re}\left[\gamma_{c,12}^{(j)}(1,s)\right]&=\mathrm{Re}\left[\gamma_{j,11}(1,s)\right]\mathrm{Re}\left[\gamma_{c,12}^{(j-1)}(s)\right]-\mathrm{Im}\left[\gamma_{j,11}(1,s)\right]\mathrm{Im}\left[\gamma_{c,12}^{(j-1)}(s)\right]\\&+\mathrm{Re}\left[\gamma_{j,12}(1,s)\right]\mathrm{Re}\left[\gamma_{c,22}^{(j-1)}(s)\right]-\mathrm{Im}\left[\gamma_{j,12}(1,s)\right]\mathrm{Im}\left[\gamma_{c,22}^{(j-1)}(s)\right],\end{aligned}\tag{A3}$$

$$\begin{aligned}\mathrm{Im}\left[\gamma_{c,12}^{(j)}(1,s)\right]&=\mathrm{Im}\left[\gamma_{j,11}(1,s)\right]\mathrm{Re}\left[\gamma_{c,12}^{(j-1)}(s)\right]+\mathrm{Re}\left[\gamma_{j,11}(1,s)\right]\mathrm{Im}\left[\gamma_{c,12}^{(j-1)}(s)\right]\\&+\mathrm{Im}\left[\gamma_{j,12}(1,s)\right]\mathrm{Re}\left[\gamma_{c,22}^{(j-1)}(s)\right]+\mathrm{Re}\left[\gamma_{j,12}(1,s)\right]\mathrm{Im}\left[\gamma_{c,22}^{(j-1)}(s)\right],\end{aligned}\tag{A4}$$

$$\begin{aligned}\mathrm{Re}\left[\gamma_{c,21}^{(j)}(1,s)\right]&=\mathrm{Re}\left[\gamma_{j,21}(1,s)\right]\mathrm{Re}\left[\gamma_{c,11}^{(j-1)}(s)\right]-\mathrm{Im}\left[\gamma_{j,21}(1,s)\right]\mathrm{Im}\left[\gamma_{c,11}^{(j-1)}(s)\right]\\&+\mathrm{Re}\left[\gamma_{j,22}(1,s)\right]\mathrm{Re}\left[\gamma_{c,21}^{(j-1)}(s)\right]-\mathrm{Im}\left[\gamma_{j,22}(1,s)\right]\mathrm{Im}\left[\gamma_{c,21}^{(j-1)}(s)\right],\end{aligned}\tag{A5}$$

$$\begin{aligned}\mathrm{Im}\left[\gamma_{c,21}^{(j)}(1,s)\right]&=\mathrm{Im}\left[\gamma_{j,21}(1,s)\right]\mathrm{Re}\left[\gamma_{c,11}^{(j-1)}(s)\right]+\mathrm{Re}\left[\gamma_{j,21}(1,s)\right]\mathrm{Im}\left[\gamma_{c,11}^{(j-1)}(s)\right]\\&+\mathrm{Im}\left[\gamma_{j,22}(1,s)\right]\mathrm{Re}\left[\gamma_{c,21}^{(j-1)}(s)\right]+\mathrm{Re}\left[\gamma_{j,22}(1,s)\right]\mathrm{Im}\left[\gamma_{c,21}^{(j-1)}(s)\right],\end{aligned}\tag{A6}$$

$$\begin{aligned}\mathrm{Re}\left[\gamma_{c,22}^{(j)}(1,s)\right]&=\mathrm{Re}\left[\gamma_{j,21}(1,s)\right]\mathrm{Re}\left[\gamma_{c,12}^{(jk-1)}(s)\right]-\mathrm{Im}\left[\gamma_{j,21}(1,s)\right]\mathrm{Im}\left[\gamma_{c,12}^{(j-1)}(s)\right]\\&+\mathrm{Re}\left[\gamma_{j,22}(1,s)\right]\mathrm{Re}\left[\gamma_{c,22}^{(j-1)}(s)\right]-\mathrm{Im}\left[\gamma_{j,22}(1,s)\right]\mathrm{Im}\left[\gamma_{c,22}^{(j-1)}(s)\right],\end{aligned}\tag{A7}$$

$$\begin{aligned}\mathrm{Im}\left[\gamma_{c,22}^{(j)}(1,s)\right]&=\mathrm{Im}\left[\gamma_{j,21}(1,s)\right]\mathrm{Re}\left[\gamma_{c,12}^{(j-1)}(s)\right]+\mathrm{Re}\left[\gamma_{j,21}(1,s)\right]\mathrm{Im}\left[\gamma_{c,12}^{(j-1)}(s)\right]\\&+\mathrm{Im}\left[\gamma_{j,22}(1,s)\right]\mathrm{Re}\left[\gamma_{c,22}^{(j-1)}(s)\right]+\mathrm{Re}\left[\gamma_{j,22}(1,s)\right]\mathrm{Im}\left[\gamma_{c,22}^{(j-1)}(s)\right].\end{aligned}\tag{A8}$$

Appendix B

Following the definition of equation (29), the real and imaginary parts of the transfer function $\hat{f}_Q^{(N)}(s)$ can be calculated if the real and imaginary parts of the components of matrix $\gamma_c^{(N)}(s)$ are known (see Appendix A). It is easy to show by means of elementary complex algebra that

$$\mathrm{Re}\left[\hat{f}_Q^{(N)}(s)\right]=k_B\frac{\varphi_{1,Q}\varphi_{2,Q}+\theta_{1,Q}\theta_{2,Q}}{{\varphi_{2,Q}}^2+{\theta_{2,Q}}^2},\quad \mathrm{Im}\left[\hat{f}_Q^{(N)}(s)\right]=k_B\frac{\theta_{1,Q}\varphi_{2,Q}-\varphi_{1,Q}\theta_{2,Q}}{{\varphi_{2,Q}}^2+{\theta_{2,Q}}^2},\tag{B1}$$

where

$$\begin{aligned}\varphi_{1,Q}&=\mathrm{Re}\left[\gamma_{c,11}^{(N)}(s)\right]\mathrm{Re}\left[\gamma_{c,22}^{(N)}(s)\right]-\mathrm{Im}\left[\gamma_{c,11}^{(N)}(s)\right]\mathrm{Im}\left[\gamma_{c,22}^{(N)}(s)\right]-\mathrm{Re}\left[\gamma_{c,12}^{(N)}(s)\right]\mathrm{Re}\left[\gamma_{c,21}^{(N)}(s)\right]+\mathrm{Im}\left[\gamma_{c,12}^{(N)}(s)\right]\mathrm{Im}\left[\gamma_{c,21}^{(N)}(s)\right]\\\theta_{1,Q}&=\mathrm{Im}\left[\gamma_{c,11}^{(N)}(s)\right]\mathrm{Re}\left[\gamma_{c,22}^{(N)}(s)\right]-\mathrm{Re}\left[\gamma_{c,11}^{(N)}(s)\right]\mathrm{Im}\left[\gamma_{c,22}^{(N)}(s)\right]-\mathrm{Re}\left[\gamma_{c,12}^{(N)}(s)\right]\mathrm{Im}\left[\gamma_{c,21}^{(N)}(s)\right]-\mathrm{Im}\left[\gamma_{c,12}^{(N)}(s)\right]\mathrm{Re}\left[\gamma_{c,21}^{(N)}(s)\right],\\\varphi_{2,Q}&=k_B\mathrm{Re}\left[\gamma_{c,22}^{(N)}(s)\right]-\mathrm{Re}\left[\gamma_{c,12}^{(N)}(s)\right]\theta_{2,Q}=k_B\mathrm{Im}\left[\gamma_{c,22}^{(N)}(s)\right]-\mathrm{Im}\left[\gamma_{c,12}^{(N)}(s)\right]\end{aligned}\tag{B2}$$

The real and imaginary parts of the transfer function $\hat{g}_Q^{(N)}(s)$ are easily obtained as

$$\mathrm{Re}\left[\hat{g}_Q^{(N)}(s)\right]=\frac{1}{k_B}\mathrm{Re}\left[\hat{f}_Q^{(N)}(s)\right],\quad \mathrm{Im}\left[\hat{g}_Q^{(N)}(s)\right]=\frac{1}{k_B}\mathrm{Im}\left[\hat{f}_Q^{(N)}(s)\right]. \tag{B3}$$

Similarly, it is simple to verify that

$$\mathrm{Re}\left[\hat{f}_h^{(N)}(s)\right]=k_B\frac{\varphi_{1,h}\varphi_{2,h}+\theta_{1,h}\theta_{2,h}}{{\varphi_{2,h}}^2+{\theta_{2,h}}^2},\quad \mathrm{Im}\left[\hat{f}_h^{(N)}(s)\right]=k_B\frac{\theta_{1,h}\varphi_{2,h}-\varphi_{1,h}\theta_{2,h}}{{\varphi_{2,h}}^2+{\theta_{2,h}}^2}, \tag{B4}$$

where

$$\begin{aligned}\varphi_{1,h}&=\varphi_{1,Q}\\ \theta_{1,h}&=\theta_{1,Q}\\ \varphi_{2,h}&=\mathrm{Re}\left[\gamma_{c,11}^{(N)}(s)\right]-k_B\mathrm{Re}\left[\gamma_{c,21}^{(N)}(s)\right]\\ \theta_{2,h}&=\mathrm{Im}\left[\gamma_{c,11}^{(N)}(s)\right]-k_B\mathrm{Im}\left[\gamma_{c,21}^{(N)}(s)\right].\end{aligned} \tag{B5}$$

The real and imaginary parts of the transfer function $\hat{g}_h^{(N)}(s)$ are easily obtained as

$$\mathrm{Re}\left[\hat{g}_h^{(N)}(s)\right]=\frac{1}{k_B}\mathrm{Re}\left[\hat{f}_h^{(N)}(s)\right],\quad \mathrm{Im}\left[\hat{g}_h^{(N)}(s)\right]=\frac{1}{k_B}\mathrm{Im}\left[\hat{f}_h^{(N)}(s)\right]. \tag{B6}$$

Appendix C

Following the definition of equation (37), the transfer functions $\hat{f}_Q^{(j)}(s)$ and $\hat{g}_Q^{(j)}(s)$ can be immediately calculated if the transfer functions $\hat{f}_Q^{(j+1)}(s)$ and $\hat{g}_Q^{(j+1)}(s)$ are known:

$$\begin{bmatrix}\hat{f}_Q^{(j)}(s)\\ \hat{g}_Q^{(j)}(s)\end{bmatrix}={\gamma_{j+1}}^{-1}(1,s)\begin{bmatrix}\hat{f}_Q^{(j+1)}(s)\\ \hat{g}_Q^{(+1)}(s)\end{bmatrix},\quad j=1,2,\ldots,N-1. \tag{C1}$$

The real and imaginary parts of $\hat{f}_Q^{(j)}(s)$ and $\hat{g}_Q^{(j)}(s)$ are then expressed by:

$$\begin{aligned}\mathrm{Re}\left[\hat{f}_Q^{(j)}(s)\right]&=e^{-Pe_{j+1}}\left(\mathrm{Re}\left[\gamma_{j+1,22}(1,s)\right]\mathrm{Re}\left[\hat{f}_Q^{(j+1)}(s)\right]-\mathrm{Im}\left[\gamma_{j+1,22}(1,s)\right]\mathrm{Im}\left[\hat{f}_Q^{(j+1)}(s)\right]\right)\\ &\quad -e^{-Pe_{j+1}}\left(\mathrm{Re}\left[\gamma_{j+1,12}(1,s)\right]\mathrm{Re}\left[\hat{g}_Q^{(j+1)}(s)\right]-\mathrm{Im}\left[\gamma_{j+1,12}(1,s)\right]\mathrm{Im}\left[\hat{g}_Q^{(j+1)}(s)\right]\right)\\ \mathrm{Im}\left[\hat{f}_Q^{(j)}(s)\right]&=e^{-Pe_{j+1}}\left(\mathrm{Re}\left[\gamma_{j+1,22}(1,s)\right]\mathrm{Im}\left[\hat{f}_Q^{(j+1)}(s)\right]+\mathrm{Im}\left[\gamma_{j+1,22}(1,s)\right]\mathrm{Re}\left[\hat{f}_Q^{(j+1)}(s)\right]\right)\\ &\quad -e^{-Pe_{j+1}}\left(\mathrm{Re}\left[\gamma_{j+1,12}(1,s)\right]\mathrm{Im}\left[\hat{g}_Q^{(j+1)}(s)\right]+\mathrm{Im}\left[\gamma_{j+1,12}(1,s)\right]\mathrm{Re}\left[\hat{g}_Q^{(j+1)}(s)\right]\right)\\ \mathrm{Re}\left[\hat{g}_Q^{(j)}(s)\right]&=-e^{-Pe_{j+1}}\left(\mathrm{Re}\left[\gamma_{j+1,21}(1,s)\right]\mathrm{Re}\left[\hat{f}_Q^{(j+1)}(s)\right]-\mathrm{Im}\left[\gamma_{j+1,21}(1,s)\right]\mathrm{Im}\left[\hat{f}_Q^{(j+1)}(s)\right]\right)\\ &\quad +e^{-Pe_{j+1}}\left(\mathrm{Re}\left[\gamma_{j+1,11}(1,s)\right]\mathrm{Re}\left[\hat{g}_Q^{(j+1)}(s)\right]-\mathrm{Im}\left[\gamma_{j+1,11}(1,s)\right]\mathrm{Im}\left[\hat{g}_Q^{(j+1)}(s)\right]\right)\\ \mathrm{Im}\left[\hat{g}_Q^{(j)}(s)\right]&=-e^{-Pe_{j+1}}\left(\mathrm{Re}\left[\gamma_{j+1,21}(1,s)\right]\mathrm{Im}\left[\hat{f}_Q^{(j+1)}(s)\right]+\mathrm{Im}\left[\gamma_{j+1,21}(1,s)\right]\mathrm{Re}\left[\hat{f}_Q^{(j+1)}(s)\right]\right)\\ &\quad +e^{-Pe_{j+1}}\left(\mathrm{Re}\left[\gamma_{j+1,11}(1,s)\right]\mathrm{Im}\left[\hat{g}_Q^{(j+1)}(s)\right]+\mathrm{Im}\left[\gamma_{j+1,11}(1,s)\right]\mathrm{Re}\left[\hat{g}_Q^{(j+1)}(s)\right]\right).\end{aligned} \tag{C2}$$

Exploiting the same recursion property, it is possible to show that the real and imaginary parts of $\hat{f}_h^{(j)}(s)$ and $\hat{g}_h^{(j)}(s)$ are then expressed by:

$$
\begin{aligned}
\mathrm{Re}\left[\hat{f}_h^{(j)}(s)\right] &= e^{-Pe_{j+1}}\left(\mathrm{Re}\left[\gamma_{j+1,22}(1,s)\right]\mathrm{Re}\left[\hat{f}_h^{(j+1)}(s)\right]-\mathrm{Im}\left[\gamma_{j+1,22}(1,s)\right]\mathrm{Im}\left[\hat{f}_h^{(j+1)}(s)\right]\right)\\
&\quad -e^{-Pe_{j+1}}\left(\mathrm{Re}\left[\gamma_{j+1,12}(1,s)\right]\mathrm{Re}\left[\hat{g}_h^{(j+1)}(s)\right]-\mathrm{Im}\left[\gamma_{j+1,12}(1,s)\right]\mathrm{Im}\left[\hat{g}_h^{(j+1)}(s)\right]\right)\\
\mathrm{Im}\left[\hat{f}_h^{(j)}(s)\right] &= e^{-Pe_{j+1}}\left(\mathrm{Re}\left[\gamma_{j+1,22}(1,s)\right]\mathrm{Im}\left[\hat{f}_h^{(j+1)}(s)\right]+\mathrm{Im}\left[\gamma_{j+1,22}(1,s)\right]\mathrm{Re}\left[\hat{f}_h^{(j+1)}(s)\right]\right)\\
&\quad -e^{-Pe_{j+1}}\left(\mathrm{Re}\left[\gamma_{j+1,12}(1,s)\right]\mathrm{Im}\left[\hat{g}_h^{(j+1)}(s)\right]+\mathrm{Im}\left[\gamma_{j+1,12}(1,s)\right]\mathrm{Re}\left[\hat{g}_h^{(j+1)}(s)\right]\right)\\
\mathrm{Re}\left[\hat{g}_h^{(j)}(s)\right] &= -e^{-Pe_{j+1}}\left(\mathrm{Re}\left[\gamma_{j+1,21}(1,s)\right]\mathrm{Re}\left[\hat{f}_h^{(j+1)}(s)\right]-\mathrm{Im}\left[\gamma_{j+1,21}(1,s)\right]\mathrm{Im}\left[\hat{f}_h^{(j+1)}(s)\right]\right)\\
&\quad +e^{-Pe_{j+1}}\left(\mathrm{Re}\left[\gamma_{j+1,11}(1,s)\right]\mathrm{Re}\left[\hat{g}_h^{(j+1)}(s)\right]-\mathrm{Im}\left[\gamma_{j+1,11}(1,s)\right]\mathrm{Im}\left[\hat{g}_h^{(j+1)}(s)\right]\right)\\
\mathrm{Im}\left[\hat{g}_h^{(j)}(s)\right] &= -e^{-Pe_{j+1}}\left(\mathrm{Re}\left[\gamma_{j+1,21}(1,s)\right]\mathrm{Im}\left[\hat{f}_h^{(j+1)}(s)\right]+\mathrm{Im}\left[\gamma_{j+1,21}(1,s)\right]\mathrm{Re}\left[\hat{f}_h^{(j+1)}(s)\right]\right)\\
&\quad +e^{-Pe_{j+1}}\left(\mathrm{Re}\left[\gamma_{j+1,11}(1,s)\right]\mathrm{Im}\left[\hat{g}_h^{(j+1)}(s)\right]+\mathrm{Im}\left[\gamma_{j+1,11}(1,s)\right]\mathrm{Re}\left[\hat{g}_h^{(j+1)}(s)\right]\right).
\end{aligned}
\tag{C3}
$$

Appendix D

The unit-step responses of the nonuniform channel at the end of the subreaches can be calculated as follows:

$$
\begin{aligned}
\mathrm{Re}\left[\hat{F}_Q^{(j)}(s)\right] &= \left(\mathrm{Re}\left[\hat{f}_Q^{(j)}(s)\right]\alpha+\mathrm{Im}\left[\hat{f}_Q^{(j)}(s)\right]\omega\right)/(\alpha^2+\omega^2)\\
\mathrm{Im}\left[\hat{F}_Q^{(j)}(s)\right] &= \left(\mathrm{Im}\left[\hat{f}_Q^{(j)}(s)\right]\alpha-\mathrm{Re}\left[\hat{f}_Q^{(j)}(s)\right]\omega\right)/(\alpha^2+\omega^2)\\
\mathrm{Re}\left[\hat{G}_Q^{(j)}(s)\right] &= \left(\mathrm{Re}\left[\hat{g}_Q^{(j)}(s)\right]\alpha+\mathrm{Im}\left[\hat{g}_Q^{(j)}(s)\right]\omega\right)/(\alpha^2+\omega^2)\\
\mathrm{Im}\left[\hat{G}_Q^{(j)}(s)\right] &= \left(\mathrm{Im}\left[\hat{g}_Q^{(j)}(s)\right]\alpha-\mathrm{Re}\left[\hat{g}_Q^{(j)}(s)\right]\omega\right)/(\alpha^2+\omega^2)\\
\mathrm{Re}\left[\hat{F}_h^{(j)}(s)\right] &= \left(\mathrm{Re}\left[\hat{f}_h^{(j)}(s)\right]\alpha+\mathrm{Im}\left[\hat{f}_h^{(j)}(s)\right]\omega\right)/(\alpha^2+\omega^2)\\
\mathrm{Im}\left[\hat{F}_h^{(j)}(s)\right] &= \left(\mathrm{Im}\left[\hat{f}_h^{(j)}(s)\right]\alpha-\mathrm{Re}\left[\hat{f}_h^{(j)}(s)\right]\omega\right)/(\alpha^2+\omega^2)\\
\mathrm{Re}\left[\hat{G}_h^{(j)}(s)\right] &= \left(\mathrm{Re}\left[\hat{g}_h^{(j)}(s)\right]\alpha+\mathrm{Im}\left[\hat{g}_h^{(j)}(s)\right]\omega\right)/(\alpha^2+\omega^2)\\
\mathrm{Im}\left[\hat{G}_h^{(j)}(s)\right] &= \left(\mathrm{Im}\left[\hat{g}_h^{(j)}(s)\right]\alpha-\mathrm{Re}\left[\hat{g}_h^{(j)}(s)\right]\omega\right)/(\alpha^2+\omega^2),
\end{aligned}
\tag{D1}
$$

where α and ω are the real and imaginary parts of s, respectively.

Acknowledgments
The writers want to acknowledge the Editor, the Associate Editor, and the three anonymous Reviewers, for having contributed to improve the paper with their constructive criticisms. All the data used for the tests are available from the cited references.

References

Becker, A., and Z. W. Kundzewicz (1987), Nonlinear flood routing with multilinear models, *Water Resour. Res.*, *23*(6), 1043–1048.
Camacho, L. A., and M. J. Lees (1999), Multilinear discrete lag-cascade model for channel routing, *J. Hydrol.*, *226*(1–2), 30–47.
Chow, V. T., D. R. Maidment, and L. W. Mays (1988), *Applied Hydrology*, McGraw-Hill, N. Y.
Chung, W. H., A. A. Aldama, and J. A. Smith (1993), On the effects of downstream boundary conditions on diffusive flood routing, *Adv. Water Resour.*, *16*, 259–275.
Cimorelli, L., L. Cozzolino, C. Covelli, C. Mucherino, A. Palumbo, and D. Pianese (2013a), Optimal design of rural drainage networks, *J. Irrig. Drain. Eng.*, *139*(2), 137–144.
Cimorelli, L., L. Cozzolino, R. Della Morte, and D. Pianese (2013b), An improved numerical scheme for the approximate solution of the Parabolic Wave model, *J. Hydroinformatics*, *15*(3), 913–925.
Cimorelli, L., L. Cozzolino, R. Della Morte, and D. Pianese (2014a), Analytical solutions of the linearized parabolic wave accounting for downstream boundary condition and uniform lateral inflows, *Adv. Water Resour.*, *63*, 57–76.
Cimorelli, L., L. Cozzolino, C. Covelli, R. Della Morte, and D. Pianese (2014b), Enhancing the efficiency of the automatic design of rural drainage networks, *J. Irrig. Drain. Eng.*, *140*(6), 04014015.
Cohen, A. M. (2007), *Numerical Methods for Laplace Transform Inversion*, vol. 5, Springer, N. Y.
Cozzolino, L., R. Della Morte, G. Del Giudice, A. Palumbo, and D. Pianese (2012), A well-balanced spectral volume scheme with the wetting–drying property for the shallow-water equations, *J. Hydroinformatics*, *14*(3), 745–760.
Cozzolino, L., L. Cimorelli, C. Covelli, R. Della Morte, and D. Pianese (2014a), Boundary conditions in finite volume schemes for the solution of shallow-water equations: The non-submerged broad-crested weir, *J. Hydroinformatics*, *16*(6), 1235–1249.
Cozzolino, L., R. Della Morte, L. Cimorelli, C. Covelli, and D. Pianese (2014b), A broad-crested weir boundary condition in finite volume shallow-water numerical models, *Procedia Eng.*, *70*, 353–362.

Cozzolino, L., L. Cimorelli, C. Covelli, C. Mucherino, and D. Pianese (2015), An innovative approach for drainage network sizing, *Water*, *7*(2), 546–567.
Crump, K. S. (1976), Numerical inversion of Laplace transforms using a Fourier series approximation, *J. Assoc. Comput. Mach.*, *23*(1), 89–96.
Cunge, J., F. M. Holly, and A. Verwey (1980), *Practical Aspects of Computational River Hydraulics*, Advanced Publishing Program, Pitman, London, U. K.
Cunge, J. A. (1969), On the subject of a flood propagation computation method (Muskingum Method), *J. Hydraul. Res.*, *7*(2), 205–230.
Hayami, S. (1951), On the propagation of flood waves, *Bulletin 1*, pp. 1–16, Disaster Prev. Res. Inst., Kyoto Univ., Kyoto, Japan.
Kalinin, G. P., and P. I. Milyukov (1957), O raschete neustanovivshegosya dvizheniya vody v otkrytykh ruslakh [in Russian], *Meteorol. Gydrol. Zh.*, *10*, 10–18.
Keefer, T. N., and R. S. McQuivey (1974), Multiple linearization flow routing model, *J. Hydraul. Div.*, *100*(HY7), 1031–1046.
Litrico, X., and V. Fromion (2004), Frequency modeling of open-channel flow, *J. Hydraul. Eng.*, *130*(8), 806–815.
Litrico, X., J. B. Pomet, and V. Guinot (2010), Simplified nonlinear modeling of river flow routing, *Adv. Water Resour.*, *33*(9), 1015–1023.
Munier, S., X. Litrico, G. Belaud, and P. O. Malaterre (2008), Distributed approximation of open-channel flow routing accounting for backwater effects, *Adv. Water Resour.*, *31*(12), 1590–1602.
Nash, J. E. (1957), The form of instantaneous unit hydrograph, *Int. Assoc. Sci. Hydrol.*, *45*(3), 114–121.
Palumbo, A., L. Cimorelli, C. Covelli, L. Cozzolino, C. Mucherino, and D. Pianese (2014), Optimal design of urban drainage networks, *Civ. Eng. Environ. Syst.*, *31*(1), 79–96.
Perumal, M. (1992), Multilinear Muskingum flood routing method, *J. Hydrol.*, *133*(3), 259–272.
Perumal, M. (1994), Multilinear discrete cascade model for channel routing, *J. Hydrol.*, *158*(1–2), 135–150.
Perumal, M., T. Moramarco, B. Sahoo, and S. Barbetta (2007), A methodology for discharge estimation and rating curve development at ungaged river sites, *Water Resour. Res.*, *43*, W02412, doi:10.1029/2005WR004609.
Perumal, M., B. Sahoo, T. Moramarco, and S. Barbetta (2009), Multilinear Muskingum method for stage-hydrograph routing in compound channels, *J. Hydrol. Eng.*, *14*(7), 663–670.
Ponce, V. M., and D. B. Simmons (1977), Shallow wave propagation in open channel flow, *J. Hydraul. Div.*, *103*(HY12), 1461–1476.
Ponce, V. M., and V. Yevjevich (1978), Muskingum–Cunge method with variable parameters, *J. Hydraul. Div.*, *104*(HY12), 1663–1667.
Ponce, V. M., R.-M. Li, and D. B. Simmons (1978), Applicability of kinematic and diffusion models, *J. Hydraul. Div.*, *104*(HY3), 353–360.
Rashid, R. S. M. M., and M. H. Chaudhry (1995), Flood routing in channels with floodplains, *J. Hydrol.*, *171*, 75–91.
Singh, V. P. (1996), *Kinematic Wave Modeling in Water Resources: Surface Water Hydrology*, John Wiley, N. Y.
Singh, V. P., and D. A. Woolhiser (1976), A non-linear kinematic wave model for catchment surface runoff, *J. Hydrol.*, *31*, 221–243.
Szilagyi, J. (2003), State-space discretization of the Kalinin-Milyukov-Nash-Cascade in a sample-data system framework for streamflow forecasting, *J. Hydrol. Eng.*, *8*(6), 339–347.
Szilagyi, J. (2006), Discrete state-space approximation of the continuous Kalinin–Milyukov–Nash cascade of noninteger storage elements, *J. Hydrol.*, *328*(1), 132–140.
Szilagyi, J., and P. Laurinyecz (2012), Accounting for backwater effects in flow routing by the discrete linear cascade model, *J. Hydrol. Eng.*, *19*(1), 69–77.
Todini, E., and A. Bossi(1986), PAB (Parabolic and Backwater), an unconditionally stable flood routing scheme particularly suited for real time forecasting and control, *J. Hydraul. Res.*, *24*(5), 405–424.
Tsai, C. W. (2003), Applicability of kinematic, noninertia, and quasi-steady gynamic wave models to unsteady flow routing, *J. Hydraul. Eng.*, *129*(8), 613–627.
Tsai, C. W. (2005), Flood routing in mild-slope rivers–wave characteristics and downstream backwater effect, *J. Hydrol.*, *308*, 151–167.
Weinmann, P. E., and E. M. Laurenson (1979), Approximate flood routing methods: A review, *J. Hydraul. Div.*, *105*(HY12), 1521–1526.
Wynn, P. (1962), Acceleration techniques for iterative vector problems, *Math. Comput.*, *16*, 301–322.